DE GRUYTER OPEN

Int. J. of Applied Mechanics and Engineering, 2017, vol.22, No.1, pp.145-161
DOI: 10.1515/ijame-2017-0009

UNSTEADY MHD HEAT TRANSFER IN COUETTE FLOW OF WATER AT $4^{O}C$ IN A ROTATING SYSTEM WITH RAMPED TEMPERATURE VIA FINITE ELEMENT METHOD

G.J. REDDY*
Department of Humanities and Sciences
VNR Vignana Jyothi Institute of Engineering & Technology
Bachupally, Hyderabad, 500090, Telangana State, INDIA
E-mail addresses: jithendergurejala@gmail.com

R.S. RAJU
Department of Mathematics, GITAM University
Hyderabad Campus, Rudraram, 502329, Telangana State, INDIA

J.A. RAO
Department of Mathematics, Faculty of Science
Osmania University
Hyderabad, 500007, Telangana State, INDIA

R.S.R. GORLA
Department of Mechanical & Civil Engineering
Purdue University Northwest
Westville, Indiana 46391 USA

An unsteady magnetohydromagnetic natural convection on the Couette flow of electrically conducting water at 4^0C (Pr = 11.40) in a rotating system has been considered. A Finite Element Method (FEM) was employed to find the numerical solutions of the dimensionless governing coupled boundary layer partial differential equations. The primary velocity, secondary velocity and temperature of water at 4^oC as well as shear stresses and rate of heat transfer have been obtained for both ramped temperature and isothermal plates. The results are independent of the mesh (grid) size and the present numerical solutions through the Finite Element Method (FEM) are in good agreement with the existing analytical solutions by the Laplace Transform Technique (LTT). These are shown in tabular and graphical forms.

Key words: MHD, Couette flow, heat transfer, FEM.

1. Introduction

The effects of 4^oC on the natural convective heat transfer and temperature distribution with initial temperatures at 4^oC and 8^oC were reported by Forbes and Cooper [1] who cooled water from the top with either a rigid boundary condition at constant temperature or a free water-air surface with a constant convective heat transfer coefficient. We known that for a fluid like water or air at ordinary temperature and atmospheric pressure the variation $\Delta\rho$ of the density with the variation $\Delta T'$ of the temperature is given by

$$\Delta\rho = -\rho\beta\Delta T' \tag{1.1}$$

where $\beta = 2.07\times 10^{-4}\left({}^{o}C\right)^{-1}$ at $20^{o}C$.

* To whom correspondence should be addressed

However, for temperature variations of magnitude $\pm 4°C$ away from $4°C$, the variations in the density are very closely given by

$$\Delta\rho = -\rho\gamma\left(\Delta T'\right)^2 \tag{1.2}$$

where $\gamma = 8.0 \times 10^{-6}\left({}^{o}C\right)^{-2}$.

From the above it is apparent that for low temperature variations, natural convection in water near $4°C$ would be different from that at $20°C$ [2]. Bejan and Lankford [3] investigated natural convection in a vertical enclosure filled with water near $4^{o}C$. Khan and Gorla [4] studied non similar solutions of mixed convection of water at $4°C$ on a vertical surface with a prescribed heat flux in a porous medium by an implicit finite difference method (IFDM). Khan and Gorla [5] investigated the numerical solutions of mixed convection, both free and forced convection of water at $4°C$ along a plate or wedge in a porous medium with the influence of variable surface temperature. Gorla and Stratman [6] studied an axisymmetric natural convection boundary layer flow of water at $4°C$ past slender bodies. Guedda *et al*. [7] studied an analytical solutions of MHD mixed convection on a vertical flat plate embedded in a porous medium saturated with water at $4°C$. Michalis *et al*. [8] found the numerical solutions of an MHD free convective flow of water near $4°C$ past a straight up moving plate with constant suction. Sharma *et al*. [9] studied the mixed convection steady flow of water $4°C$ along a moving non-isothermal vertical plate with the influence of a magnetic field. Ramesh *et al*. [10] presented numerical solutions for a steady two-dimensional boundary layer flow of a viscous dusty fluid over a stretching sheet with the bottom surface of the sheet heated by convection from a hot fluid. The effect of the convective boundary condition on a boundary layer stagnation-point flow of a Williamson nanofluid on a linear stretching/shrinking sheet was studied by Gorla and Gireesha [11]. Darvishi *et al.* [12] studied the effects of transient thermal performance of a rectangular porous fin in the presence of radiation by considering natural convection heat transfer using Darcy's model to formulate the heat transfer equation. Gireesha *et al*. [13] investigated the effects of Hall current, thermal radiation and non-uniform heat source/sink on hydromagnetic heat transfer in a dusty viscous fluid on a continuously stretching non-isothermal surface, with linear variation of surface temperature or heat flux. Mukhopadhyay and Gorla [14] presented an analysis to describe the boundary layer flow and heat transfer towards a porous exponential stretching sheet by considering velocity and thermal slips boundary conditions. Siddiqa *et al*. [15] studied the conjugate natural convection flow over a finite vertical surface with radiation by considering Rosseland diffusion approximation. A boundary layer analysis was presented by Singh and Gorla [16] for the combined effects of viscous dissipation, Joule heating, transpiration, heat source, thermal diffusion and Hall current on the hydromagnetic free convection and mass transfer flow of a homogeneous, incompressible fluid past an infinite vertical porous plate. The boundary layer flow of a viscous incompressible fluid due to a porous vertical stretching surface with a power-law stretching velocity in a thermally stratified medium was presented numerically by Mukhopadhyay *et al.* [17]. Bakier and Gorla [18] dealt with the thermophoresis particle deposition and thermal radiation effects on heat and mass transfer flow characteristics in a viscous fluid over a semi-infinite vertical porous plate. The influence of radiation and buoyancy on heat and mass transfer characteristics of continuous surfaces having a prescribed variable surface temperature and stretched with rapidly decreasing power law velocities was studied by Mohammadein *et al*. [19].

The Couette flow in fluid dynamics refers to the laminar flow of a viscous fluid in the space between two parallel plates, one of which moves relative to the other. This flow is driven by virtue of a viscous drag force acting on the fluid and the applied pressure gradient is parallel to the plates. Such flow was named in honor of Maurice Marie Alfred Couette. He was a professor of physics, French University of Angers, in the late 19th century. Shear – driven fluid motion is explained in undergraduate physics and engineering courses using Coutte flow. Couette motion finds applications in power generators, pumps, petroleum industry, polymer technology, purification of crude oil and fluid droplets sprays. This flow was analyzed by Kearsley *et al*. [20] and Singh [21]. Das *et al*. [22] studied the magnetic field impact on an unsteady MHD free convection Couette flow between the infinite horizontal parallel plates with the presence of a rotating system by the Laplace transform technique. Singh *et al*. [23] studied the influence of a rotating system on Couette flow through a porous medium. Recently, Seth *et al*. [24-25] studied the hydromagnetic free convection Couette flow between two vertical plates. Job and Gunakala [26] studied the unsteady MHD natural convection effects in Couette flow between permeable plates. Rao *et al.* [27] considered the effects of a chemical reaction with heat absorption on an unsteady MHD free convective fluid flow past a semi-infinite perpendicular plate embedded in a porous medium. Rao *et al*. [28] investigated the combined effects of heat and mass transfer on an unsteady MHD flow past a vertical oscillatory plate using the finite element method. Rao *et al*. [29] demonstrated a transient flow past an impulsively started infinite flat porous plate in a rotating fluid in the presence of a magnetic field with Hall current using the finite element technique. The influence of viscous dissipation on a free convective flow past a semi-infinite vertical plate in the presence of Soret and magnetic field was studied by Sheri and Srinivasa [30]. Sheri and Srinivasa [31] studied the effect of viscous dissipation on a transient free convection flow past an infinite vertical plate through a porous medium in the presence of a magnetic field using the finite element technique. Sivaiah and Srinivasa [32] studied the effects of Hall current and heat source on an MHD heat and mass transfer free convective flow in the presence of viscous dissipation by applying the finite element technique. Srinivasa [33] studied the combined effects of thermal-diffusion and diffusion-thermo on an unsteady free convection fluid flow past an infinite vertical porous plate in the presence of a magnetic field and chemical reaction using the finite element technique. Raju *et al*. [34] obtained numerical results for the effects of thermal radiation and heat source on an unsteady free convective flow past an infinite vertical plate with a transverse magnetic field in the presence of thermal-diffusion and diffusion-thermo. The combined effects of heat and mass transfer on an unsteady MHD natural convective flow past an infinite vertical plate embedded in a porous medium in the presence of thermal radiation and Hall current was investigated by Murthy *et al.* [35]. Rao *et al*. [36] obtained numerical results for non-linear partial differential equations of a free convective magnetohydrodynamic flow past a semi-infinite moving vertical plate with the effects of thermal radiation and viscous dissipation using the finite element technique.

In the present paper, the unsteady hydromagnetic free convection Couette flow of water at 4^oC, viscous incompressible and electrically conducting fluid in a rotating system is considered. A Finite Element Method is employed to find numerical solutions for the non-dimensional governing coupled PDEs with suitable boundary conditions. The primary, secondary velocity and temperature of water at 4^oC as well as shear stresses and rate of heat transfer have to be obtained for both ramped temperature and isothermal plates. The results are shown in graphical and tabular forms. The present numerical solutions are in good agreement with the analytical studies by Das *et al*. [22].

2. Formulation of the problem

Consider the unsteady heat transfer flow of a viscous incompressible electrically conducting fluid between two infinite parallel plates when the fluid and the plates spin or rotate in unison with uniform angular velocity Ω' about an axis normal to the plates.

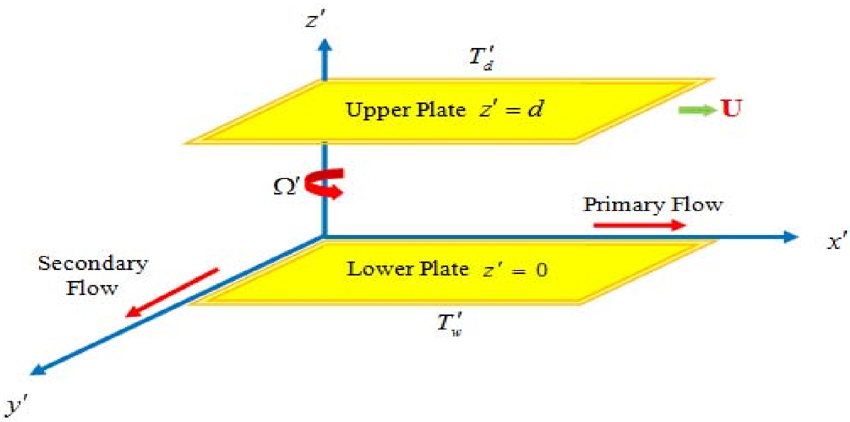

Fig.1. Geomety of the problem.

Let d be the distance between the two plates, where d is small in comparison with the characteristic length of the plates. The upper plate moves with a uniform velocity U in its own plane in the x' - direction, where the x' - axis is taken along the lower stationary plate. The z' - axis is taken normal to the x' - axis and the y' - axis is taken normal to the $x'z'$ plane, lying in the plane of the lower plate, and it is assumed that the flow is fully developed. Further, there is no applied pressure gradient as the flow is due to the motion of the upper plate. Also, assume that initially, i.e., at time $t' \le 0$, both the fluid and plates of the channel are at rest and maintained at a uniform temperature T'_d. At time $t' > 0$, the plates start moving in the z' - direction with uniform velocity U in the $x'y'$ plane. The temperature of the plate is raised or lowered to $T'_d + (T'_w - T'_d)t'/t_0$ when $0 < t' \le t_0$, and maintained uniform temperature T'_w when $t' > t_0$ (t_0 is characteristic time). Since the plates are infinitely long along the x' and y' directions, all physical quantities will be functions of z' and t' only. Denoting the velocity components u' and w' along the x' and y' directions, respectively, the Navier-Stokes equations of motion in a rotating frame of reference are

$$\frac{\partial u'}{\partial t'} = \nu \frac{\partial^2 u'}{\partial z'^2} + 2\Omega' w' - \frac{\sigma B_o^2 u'}{\rho} + g\beta\left(T' - T'_d\right), \tag{2.1}$$

$$\frac{\partial w'}{\partial t'} = \nu \frac{\partial^2 w'}{\partial z'^2} - 2\Omega' u' - \frac{\sigma B_o^2 w'}{\rho}, \tag{2.2}$$

$$\frac{\partial T'}{\partial t'} = \frac{k}{\rho c_p} \frac{\partial^2 T'}{\partial z'^2}. \tag{2.3}$$

The boundary conditions for the primary and secondary velocity and temperature are

$$\forall t' \le 0 : u' = w' = 0, \quad T' = T'_d \quad \text{for} \quad z' \ge 0, \tag{2.4}$$

$$\forall t' > 0 : \; u' = w' = 0 \quad \text{at} \quad z' = 0, \tag{2.5}$$

$$T' = T'_d + (T'_w - T'_d)t'/t_0 \quad \text{at} \quad z' = 0 \quad \text{for} \quad 0 < t' \le t_0, \tag{2.6}$$

$$\forall t' > t_0 : T' = T'_w \quad \text{at} \quad z' = 0, \tag{2.7}$$

$$\forall t' > 0 : u' = U, \quad w' = 0, \quad T' \to T'_d \quad \text{at} \quad z' = d. \tag{2.8}$$

We introduce the following non-dimensional quantities into Eqs (2.1)-(2.3) and (2.4)-(2.8)

$$u = \frac{u'}{U}, \quad w = \frac{w'}{U}, \quad \eta = \frac{z'}{d}, \quad t = \frac{\nu t'}{d^2}, \quad \theta = \frac{T' - T'_d}{T'_w - T'_d}, \quad M^2 = \frac{\sigma B_0^2 d^2}{\rho\nu},$$
$$\Omega^2 = \frac{\Omega' d^2}{\nu}, \quad \mathrm{Gr} = \frac{g\beta d^2\left(T'_w - T'_d\right)}{\nu U}, \quad \Pr = \frac{\nu\rho c_p}{k}, \quad t_o = \frac{d^2}{\nu}. \tag{2.9}$$

We obtain the non-dimensional governing equations

$$\frac{\partial u}{\partial t} = \frac{\partial^2 u}{\partial \eta^2} + 2\Omega^2 w - M^2 u + \mathrm{Gr}\theta, \tag{2.10}$$

$$\frac{\partial w}{\partial t}=\frac{\partial^2 w}{\partial \eta^2}-2\Omega^2 u-M^2 w, \tag{2.11}$$

$$\frac{\partial \theta}{\partial t}=\frac{1}{\Pr}\frac{\partial^2 \theta}{\partial \eta^2}. \tag{2.12}$$

The non-dimensional initial and boundary conditions are

$$\forall t \le 0: u=w=0, \quad \theta=0 \quad \text{for} \quad \eta \ge 0, \tag{2.13}$$

$$\forall t > 0: \; u=0, \quad w=0 \quad \text{at} \quad \eta=0, \tag{2.14}$$

$$\forall 0 < t \le 1: \theta=t \quad \text{at} \quad \eta=0, \tag{2.15}$$

$$\forall t > 1: \theta=1 \quad \text{at} \quad \eta=0, \tag{2.16}$$

$$\forall t > 0: u=1, \quad w=0, \quad \theta=0 \quad \text{at} \quad \eta=1. \tag{2.17}$$

3. Numerical solution by FEM and study of grid independence

3.1. Finite Element Method (FEM)

The finite element method (FEM) is an efficient numerical and computational method for solving a variety of engineering and real world problems, such as solid mechanics [37], stress analysis [38], heat transfer with fluids [39], aerospace [40], aircraft wing structures [41], structural engineering [42], biomaterials [43], chemical processing [44], rigid body dynamics [45], electrical analysis [46-48] and other areas. It is recognized by many researchers, developers and users as one of the most powerful numerical analysis tools ever devised to analyze complex problems of engineering. The complexity of the method, its simplicity, accuracy and computability all make it a widely used tool in modelling and design process [49]. The code or programming of the Finite element Method is less complicated than many of the spreadsheet and word processing packages found on modern microcomputers. The primary feature of FEM ([50], [51] and [52]) is its ability to describe the geometry of the problem being analyzed with great flexibility. This is because discretization of the domain of the problem is performed using highly flexible elements or uniform or non-uniform patches. The steps in the finite element analysis are as follows.

Step 1: Discretization of the Domain: The basic concept of the FEM is to divide the domain or region of the problem into small connected patches, called finite elements. A collection of elements is called a finite element mesh. These finite elements are connected in a non overlapping manner, such that they completely cover the entire space of the problem.

Step 2: Generation of Element Equations:

i) A typical element is isolated from the mesh and the variational formulation of the given problem is constructed over the typical element.
ii) Over an element, an approximate solution of the variational problem is supposed, and by substituting this in the system, the element equations are generated.
iii) The element matrix, which is also known as the stiffness matrix, is constructed by using the element interpolation functions.

Step 3: Assembly of Element Equations: The algebraic equations so obtained are assembled by imposing the inter element continuity conditions. This yields a large number of algebraic equations known as the global finite element model, which governs the whole domain.

Step 4: Imposition of Boundary Conditions: The physical boundary conditions defined in Eq.(2.12) are imposed on the assembled equations.

Step 5: Solution of Assembled Equations: The assembled equations so obtained can be solved by any of the numerical techniques, namely, the Gauss elimination method, LU decomposition method, and the final matrix equation can be solved by a direct or indirect (iterative) method. For computational purposes, the coordinate ' η ' is varied from 0 to $\eta_{\max} = 1$, i.e., external to the momentum and energy boundary layers. The whole domain is divided into a set of 100 line segments of equal width 0.1, each element being two-nodded.

Variational formulation: The variational formulation associated with Eqs (2.9)-(2.11) over a typical two-nodded linear element (η_e, η_{e+1}) is given by

$$\int_{\eta_e}^{\eta_{e+1}} w_1\left[\left(\frac{\partial u}{\partial t}\right)-\left(\frac{\partial^2 u}{\partial \eta^2}\right)-2\Omega^2 w+M^2 u-\mathrm{Gr}\theta\right]d\eta=0\,, \tag{3.1}$$

$$\int_{\eta_e}^{\eta_{e+1}} w_2\left[\left(\frac{\partial u}{\partial t}\right)-\left(\frac{\partial^2 w}{\partial \eta^2}\right)+2\Omega^2 u+M^2 w\right]d\eta=0\,, \tag{3.2}$$

$$\int_{\eta_e}^{\eta_{e+1}} w_3\left[\left(\frac{\partial \theta}{\partial t}\right)-\frac{1}{\mathrm{Pr}}\left(\frac{\partial^2 \theta}{\partial \eta^2}\right)\right]d\eta=0 \tag{3.3}$$

where w_1, w_2 and w_3 are arbitrary test functions and may be viewed as the variation in u, w and θ respectively. After reducing the order of integration and non-linearity, we arrive at the following system of equations

$$\int_{\eta_e}^{\eta_{e+1}}\left[\begin{array}{l}(w_1)\left(\frac{\partial u}{\partial t}\right)-\left(\frac{\partial w_1}{\partial \eta}\right)\left(\frac{\partial u}{\partial \eta}\right)-2(w_1)\left(\Omega^2\right)w+ \\ +\left(M^2\right)(w_1)u-(\mathrm{Gr})(w_1)\theta\end{array}\right]d\eta-\left[(w_1)\left(\frac{\partial u}{\partial \eta}\right)\right]_{\eta_e}^{\eta_{e+1}}=0\,, \tag{3.4}$$

$$\begin{array}{l}\int_{\eta_e}^{\eta_{e+1}}\left[(w_2)\left(\frac{\partial w}{\partial t}\right)-\left(\frac{\partial w_2}{\partial \eta}\right)\left(\frac{\partial w}{\partial \eta}\right)+2(w_2)\left(\Omega^2\right)u+\left(M^2\right)(w_2)w\right]d\eta+ \\ -\left[(w_2)\left(\frac{\partial w}{\partial \eta}\right)\right]_{\eta_e}^{\eta_{e+1}}=0,\end{array}\,, \tag{3.5}$$

$$\int_{\eta_e}^{\eta_{e+1}}\left[(w_3)\left(\frac{\partial \theta}{\partial t}\right)+\frac{1}{\mathrm{Pr}}\left(\frac{\partial w_3}{\partial \eta}\right)\left(\frac{\partial \theta}{\partial \eta}\right)\right]d\eta-\left[\left(\frac{w_3}{\mathrm{Pr}}\right)\left(\frac{\partial \theta}{\partial \eta}\right)\right]_{\eta_e}^{\eta_{e+1}}=0\,. \tag{3.6}$$

Finite Element formulation

The finite element model may be obtained from Eqs (3.4)-(3.6) by substituting finite element approximations of the form

$$u=\sum_{j=1}^{2} u_j^e \psi_j^e, \qquad w=\sum_{j=1}^{2} w_j^e \psi_j^e, \qquad \theta=\sum_{j=1}^{2} \theta_j^e \psi_j^e\,, \tag{3.7}$$

with $w_1 = w_2 = w_3 = \psi_j^e$ $(i = 1, 2)$, where u_j^e, w_j^e and θ_j^e are the primary velocity, secondary velocity and temperature, respectively, at the j^{th} node of typical e^{th} element (η_e, η_{e+1}) and ψ_i^e $(i = 1, 2)$ are the shape functions for this element (η_e, η_{e+1}) and are taken as

$$\psi_1^e = \frac{\eta_{e+1} - \eta}{\eta_{e+1} - \eta_e} \quad \text{and} \quad \psi_2^e = \frac{\eta - \eta_e}{\eta_{e+1} - \eta_e}, \quad \eta_e \le \eta \le \eta_{e+1}. \tag{3.8}$$

The finite element model of the equations for e^{th} element thus formed is given by

$$\begin{bmatrix} [K^{11}] & [K^{12}] & [K^{13}] \\ [K^{21}] & [K^{22}] & [K^{23}] \\ [K^{31}] & [K^{32}] & [K^{33}] \end{bmatrix} \begin{bmatrix} \{u^e\} \\ \{w^e\} \\ \{\theta^e\} \end{bmatrix} + \begin{bmatrix} [M^{11}] & [M^{12}] & [M^{13}] \\ [M^{21}] & [M^{22}] & [M^{23}] \\ [M^{31}] & [M^{32}] & [M^{33}] \end{bmatrix} \begin{bmatrix} \{u'^e\} \\ \{w'^e\} \\ \{\theta'^e\} \end{bmatrix} = \begin{bmatrix} \{b^{1e}\} \\ \{b^{2e}\} \\ \{b^{3e}\} \end{bmatrix} \tag{3.9}$$

where $\{[K^{mn}], [M^{mn}]\}$ and $\{\{u^e\}, \{w^e\}\{\theta^e\}, , \{u'^e\}, \{w'^e\} \{\theta'^e\} \text{and } \{b^{me}\}\}$ $(m, n = 1, 2, 3)$ are the set of matrices of order 2×2 and 2×1, respectively, and $'$ (dash) indicates $\frac{d}{dt}$. These matrices are defined as follows

$$K_{ij}^{11} = \int_{\eta_e}^{\eta_{e+1}} \left[\left(\frac{\partial \psi_i^e}{\partial \eta} \right) \left(\frac{\partial \psi_j^e}{\partial \eta} \right) \right] d\eta + \left(M^2 \right) \int_{\eta_e}^{\eta_{e+1}} \left(\psi_i^e \right) \left(\psi_j^e \right) dy, \quad K_{ij}^{12} = \Omega^2 \int_{\eta_e}^{\eta_{e+1}} \left(\psi_i^e \right) \left(\psi_j^e \right) d\eta,$$

$$K_{ij}^{13} = -\text{Gr} \int_{\eta_e}^{\eta_{e+1}} \left(\psi_i^e \right) \left(\psi_j^e \right) d\eta, \quad M_{ij}^{11} = \int_{\eta_e}^{\eta_{e+1}} \left(\psi_i^e \right) \left(\psi_j^e \right) d\eta, \quad M_{ij}^{12} = M_{ij}^{13} = 0,$$

$$b_i^{1e} = \left[\left(\psi_i^e \right) \left(\frac{\partial u}{\partial \eta} \right) \right]_{\eta_e}^{\eta_{e+1}}, \quad K_{ij}^{21} = -\Omega^2 \int_{\eta_e}^{\eta_{e+1}} \left(\psi_i^e \right) \left(\psi_j^e \right) d\eta,$$

$$K_{ij}^{22} = \int_{\eta_e}^{\eta_{e+1}} \left[\left(\frac{\partial \psi_i^e}{\partial \eta} \right) \left(\frac{\partial \psi_j^e}{\partial \eta} \right) \right] d\eta + \left(M^2 \right) \int_{\eta_e}^{\eta_{e+1}} \left(\psi_i^e \right) \left(\psi_j^e \right) d\eta, \quad K_{ij}^{23} = 0, \quad K_{ij}^{31} = 0, \quad K_{ij}^{32} = 0,$$

$$K_{ij}^{33} = \frac{1}{\text{Pr}} \int_{\eta_e}^{\eta_{e+1}} \left[\left(\frac{\partial \psi_i^e}{\partial \eta} \right) \left(\frac{\partial \psi_j^e}{\partial \eta} \right) \right] d\eta, \quad b_i^{2e} = \left[\left(\psi_i^e \right) \left(\frac{\partial w}{\partial \eta} \right) \right]_{\eta_e}^{\eta_{e+1}}, \quad M_{ij}^{21} = M_{ij}^{23} = 0,$$

$$M_{ij}^{22} = \int_{\eta_e}^{\eta_{e+1}} \left(\psi_i^e \right) \left(\psi_j^e \right) d\eta, \quad b_i^{3e} = \left[\left(\frac{\psi_i^e}{\text{Pr}} \right) \left(\frac{\partial \theta}{\partial \eta} \right) \right]_{\eta_e}^{\eta_{e+1}}, \quad M_{ij}^{31} = M_{ij}^{32} = 0,$$

$$M_{ij}^{33} = \int_{\eta_e}^{\eta_{e+1}} \left(\psi_i^e \right) \left(\psi_j^e \right) d\eta.$$

In a one-dimensional space, a linear element, quadratic element, or element of higher order can be taken. The entire flow domain is divided into 10000 quadratic elements of equal size. Each element is three-noded, and therefore the whole domain contains 20001 nodes. At each node, four functions are to be evaluated; hence, after assembly of the element equations, we obtain a system of 80004 equations which are nonlinear. Therefore, an iterative scheme must be utilized in the solution. After imposing the boundary conditions, a system of equations was obtained which is solved by the Gauss elimination method while maintaining an accuracy of 0.00001. A convergence criterion based on the relative difference between the current and previous iterations is employed. When these differences satisfy the desired accuracy, the solution is assumed to have been converged and the iterative process is terminated. The Gaussian quadrature is implemented for solving the integrations. The code of the algorithm was executed in MATLAB. Excellent convergence was achieved for all the results.

Table 1. The numerical values of u, w and θ for variation of mesh sizes.

	Mesh (Grid) Size = *0.01*			**Mesh (Grid) Size = *0.001***			**Mesh (Grid) Size = *0.0001***		
	u	***w***	**θ**	***u***	***w***	**θ**	***u***	***w***	**θ**
	0.000000	*0.000000*	*1.000000*	*0.000000*	*0.000000*	*1.000000*	*0.000000*	*0.000000*	*1.000000*
	0.002721	*0.254924*	*0.783725*	*0.002721*	*0.254924*	*0.783725*	*0.002721*	*0.254924*	*0.783725*
	0.006558	*0.140878*	*0.583748*	*0.006558*	*0.140878*	*0.583748*	*0.006558*	*0.140878*	*0.583748*
t=1.0	*0.012921*	*0.074854*	*0.412568*	*0.012921*	*0.074854*	*0.412568*	*0.012921*	*0.074854*	*0.412568*
	0.023358	*0.043369*	*0.275754*	*0.023358*	*0.043369*	*0.275754*	*0.023358*	*0.043369*	*0.275754*
	0.039376	*0.025887*	*0.173348*	*0.039376*	*0.025887*	*0.173348*	*0.039376*	*0.025887*	*0.173348*
	0.062678	*0.014994*	*0.102910*	*0.062678*	*0.014994*	*0.102910*	*0.062678*	*0.014994*	*0.102910*
	0.096254	*0.008123*	*0.057220*	*0.096254*	*0.008123*	*0.057220*	*0.096254*	*0.008123*	*0.057220*
	0.155346	*0.004184*	*0.029246*	*0.155346*	*0.004184*	*0.029246*	*0.155346*	*0.004184*	*0.029246*
	0.326681	*0.001787*	*0.012100*	*0.326681*	*0.001787*	*0.012100*	*0.326681*	*0.001787*	*0.012100*
	1.000000	*0.000000*	*0.000000*	*1.000000*	*0.000000*	*0.000000*	*1.000000*	*0.000000*	*0.000000*

3.2. Study of grid independence

In general, to study the grid independency/dependency, the mesh size was varied in order to check the solution at different mesh (grid) sizes . We show the numerical values of primary velocity (u), secondary velocity (w) and temperature (θ) for different values of mesh (grid) size at time $t = 1.0$ in Tab.1. From this table, we observed that there is no variation in the values of primary velocity (u), secondary velocity (w) and temperature (θ) for different values of mesh (grid) size at time $t = 1.0$. Hence, we conclude that the results are independent of the mesh (grid) size and the present numerical solutions are in excellent agreement with the existing analytical solutions, shown in Tab.2. Therefore, the Finite Element Method (FEM) is suitable to solve this type of models.

4. Skin friction, rate of heat and mass transfer

For practical engineering applications and the design of chemical engineering systems, quantities of interest include the following: the local skin-friction and the local Nusselt number which are useful to compute the shear stress and rate of heat transfer near the wall.

The skin-friction or the shear stress at the lower plate and upper plate due to primary velocity in non dimensional forms are given by

$$\tau_{x0} = \left(\frac{\partial u}{\partial \eta}\right)_{\eta=0} \quad \text{and} \quad \tau_{x1} = \left(\frac{\partial u}{\partial \eta}\right)_{\eta=1}. \tag{4.1}$$

The skin-friction or the shear stress at the lower plate and upper plate due to secondary velocity in non dimensional forms are given by

$$\tau_{y0} = \left(\frac{\partial w}{\partial \eta}\right)_{\eta=0} \quad \text{and} \quad \tau_{y1} = \left(\frac{\partial w}{\partial \eta}\right)_{\eta=1}. \tag{4.2}$$

The rate of heat transfer at the lower hot plate and upper hot plate in non-dimensional forms are given by

$$\mathrm{Nu}_o = -\left(\frac{\partial\theta}{\partial\eta}\right)_{\eta=0} \quad \text{and} \quad \mathrm{Nu}_1 = -\left(\frac{\partial\theta}{\partial\eta}\right)_{\eta=1}. \tag{4.3}$$

5. Results and discussions

The Finite Element Method was employed to solve Eqs (2.10) to (2.12) with suitable conditions. We study the effects of the Grashof number for heat transfer (Gr), magnetic field $\left(M^2\right)$, rotation $\left(\Omega^2\right)$ and Prandtl number (Pr) on the fluid velocity and temperature. These are displayed graphically against channel width variable η in Figs 2 to 11 for various values of the Grashof number for heat transfer, magnetic field parameter, rotation parameter, Prandtl number and time. Figures 2 and 3 illustrate the influence of the Grashof number on the primary and secondary velocities (u) and (w) of fluid respectively for both ramped temperature and isothermal temperature. The Grashof number for heat transfer is the relative effect of the thermal buoyancy force to the viscous hydrodynamic force in the boundary layer. As expected, it is observed that the primary velocity as well as secondary velocity (u) and (w) of the fluid increases due to the enhancement of the thermal buoyancy force for both ramped and isothermal temperature, clearly shown in Figs 2 - 3

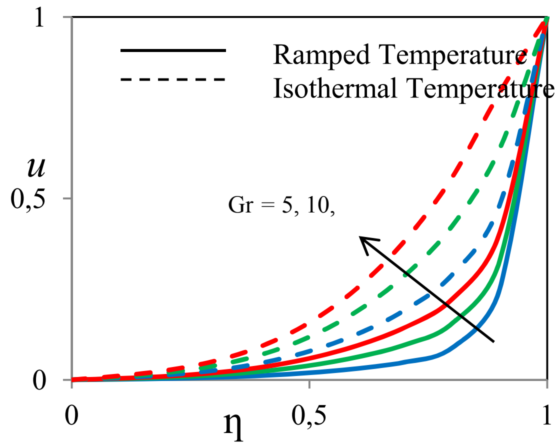

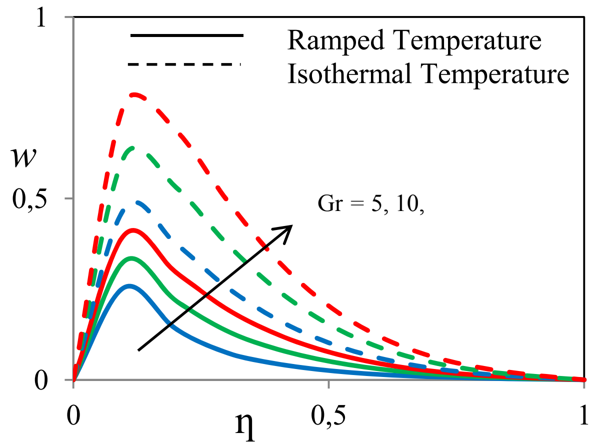

Fig.2. Influence of 'Gr' on Primary velocity profiles. Fig.3. Influence of 'Gr' on Secondary velocity profiles.

Figures 4 and 5 demonstrate the influence of the magnetic field parameter on the primary and secondary velocities (u) and (w) of the fluid respectively for both ramped temperature and isothermal plate. It is observed that the primary velocity and secondary velocity of the fluid decreases in the entire region with increasing values of the magnetic field parameter for both ramped and isothermal plates. Figures 6 and shows the effect of rotation parameter on the primary and secondary velocities (u) and (w) of the fluid respectively for both ramped temperature and isothermal conditions. The primary velocity decreases in the entire region as the rotation parameter increases while secondary velocity increases in most of the region near the stationary plate. Figures 8 and 9 show the effect of the Prandtl number on the primary and secondary velocities (u) and (w) of the fluid respectively for both ramped temperature and isothermal conditions. Both velocities decrease in the entire region between the two plates with increasing values of the Prandtl number. Figure 10 illustrates the influence of the Prandtl number on the temperature field. The temperature of the fluid decreases in the entire region with increasing values of the Prandtl number. Figure 11 depicts the influence of time on the temperature field. The temperature of the fluid increases with increasing values of the time.

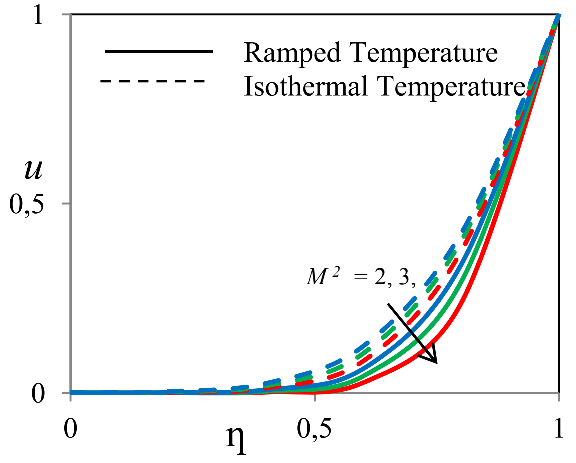

Fig.4. Influence of 'M^2' on primary velocity profiles.

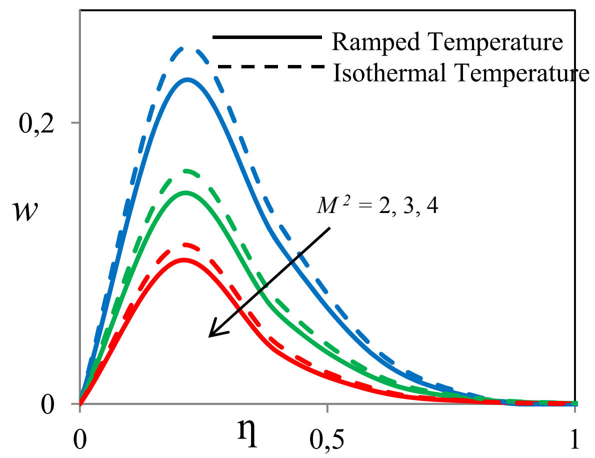

Fig.5. Influence of 'M^2' on secondary velocity profiles.

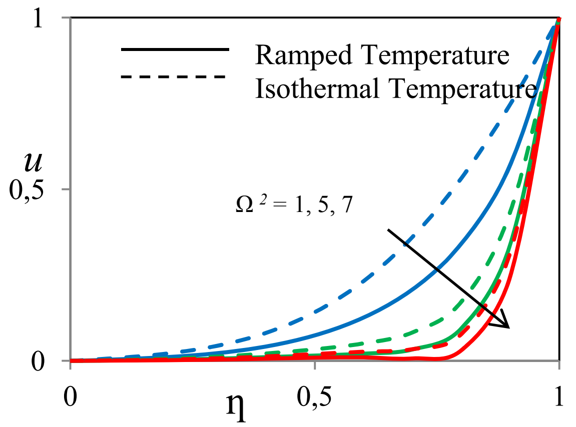

Fig.6. Influence of 'Ω^2' on primary velocity profiles.

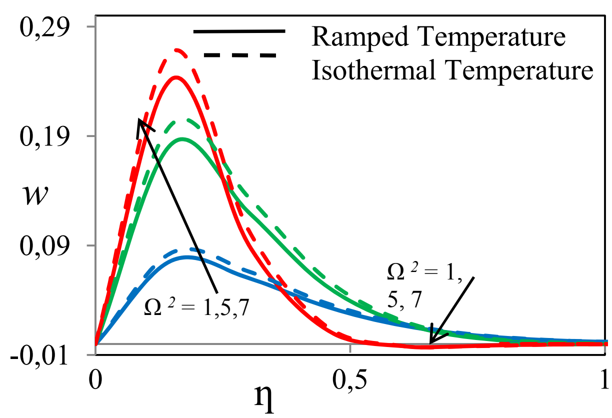

Fig.7. Influence of 'Ω^2' on secondary velocity profiles.

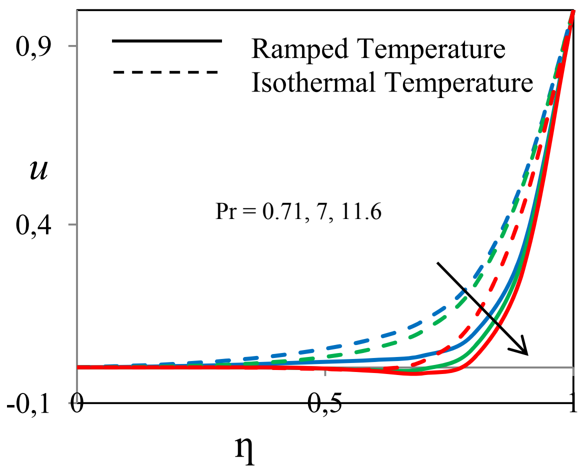

Fig.8. Influence of 'Pr' on primary velocity profiles.

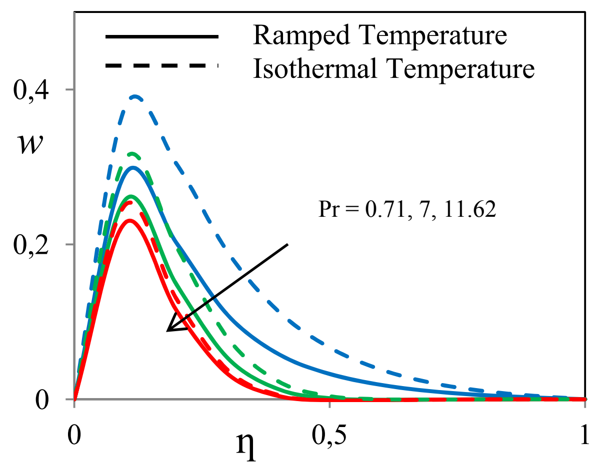

Fig.9. Influence of 'Pr' on secondary velocity profiles.

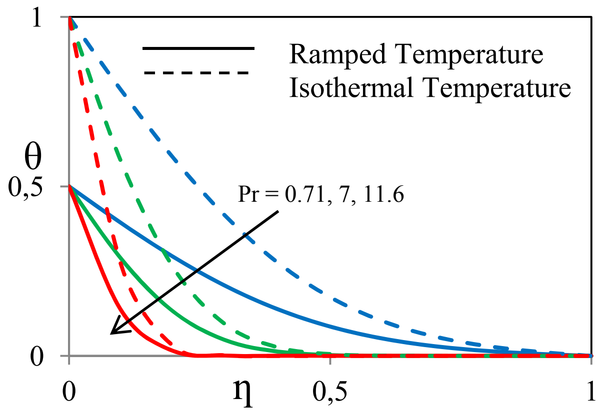

Fig.10. Influence of 'Pr' on temperature profiles.

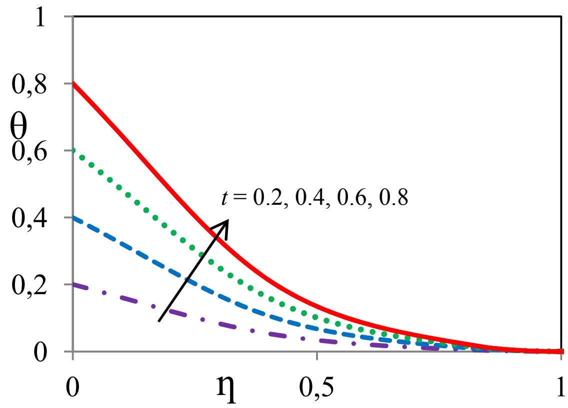

Fig.11. Influence of 't' on temperature profiles.

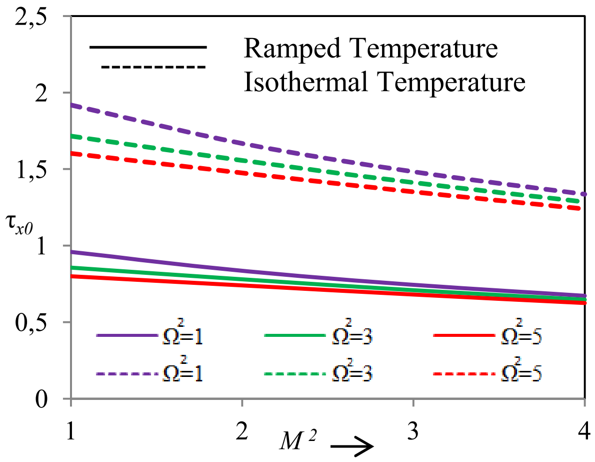

Fig.12. Shear stress at the stationary plate with various values of 'Ω^2' against the values of 'M^2' due to primary velocity.

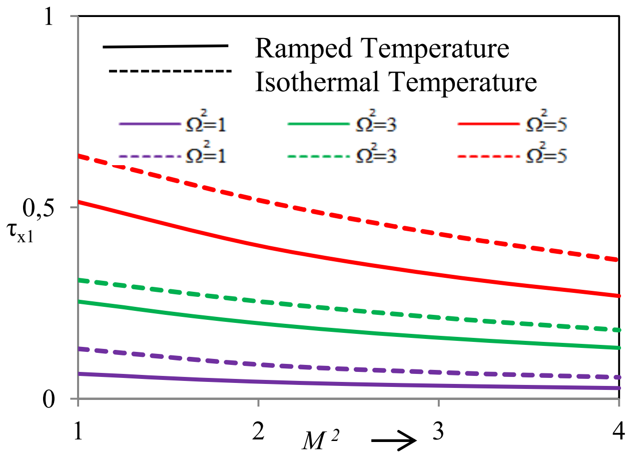

Fig.13. Shear stress at moving plate with various values of 'Ω^2' against the values of 'M^2' due to primary velocity.

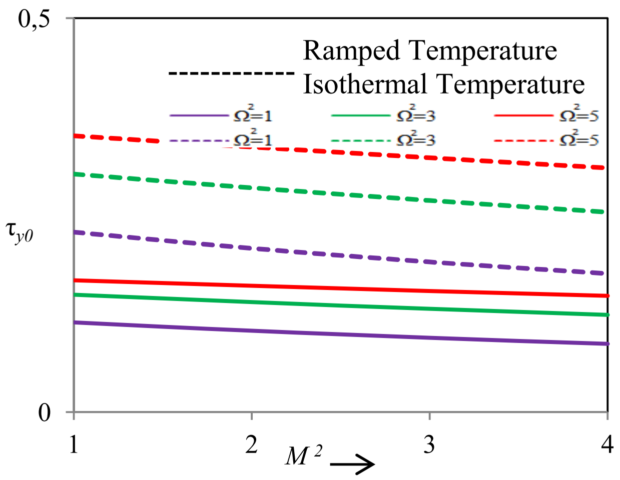

Fig.14. Shear stress at the stationary plate with various values of Ω^2 against the values of M^2 due to secondary velocity profiles.

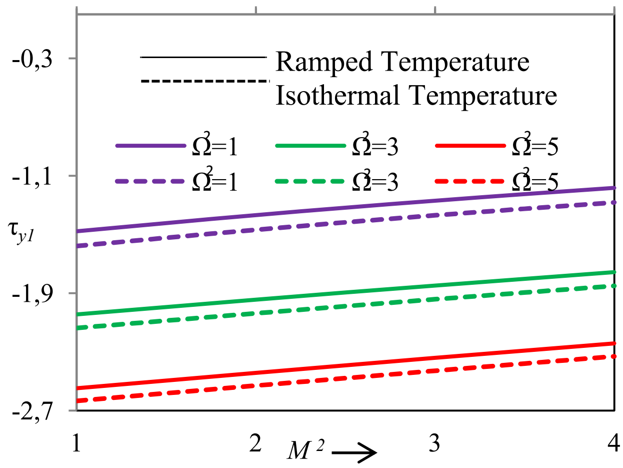

Fig.15. Shear stress at the moving plate with various values of Ω^2 against the values of M^2 due to secondary velocity profiles.

Figures 12 and 13 show the shear stress at the stationary plate $\left(\tau_{x_0}\right)$ and moving plate $\left(\tau_{x_1}\right)$ with various values of 'Ω^2' against the values of 'M^2' due to primary velocity for both ramped temperature and isothermal plates. τ_{x_0} decreases with increasing values of 'Ω^2' and 'M^2' and τ_{x_1} increases with increasing values of 'Ω^2' while decreases with increasing values of 'M^2' for both ramped temperature and isothermal plates. Figures 14 and 15 show the shear stress at the stationary plate $\left(\tau_{y_0}\right)$ and moving plate $\left(\tau_{y_1}\right)$ with various values of 'Ω^2' against the values of 'M^2' due to the secondary velocity for both ramped temperature and isothermal conditions. τ_{y_0} increases with increasing values of 'Ω^2' and decreases with increasing values of 'M^2' and τ_{y_1} increases with increasing values of 'M^2' and decreases with increasing values of 'Ω^2' for both ramped temperature and isothermal conditions. Figures 16 and 17 show the shear stress at the stationary plate $\left(\tau_{x_0}\right)$ and moving plate $\left(\tau_{x_1}\right)$ with various values of 'Pr' against the values of 'Gr' due to the primary velocity for both ramped temperature and isothermal conditions. τ_{x_0} increases with increasing values of 'Gr' and decreases with increasing values of 'Pr' and τ_{x_1} increases with increasing values of 'Pr' and for higher values of 'Gr'. It decreases for small values of 'Gr' for both ramped temperature and isothermal conditions.

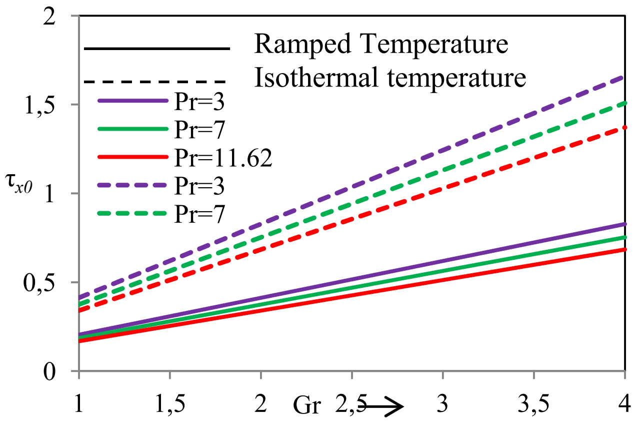

Fig.16. Shear stress at the stationary plate with various values of 'Pr' against the values of 'Gr' due to primary velocity profiles.

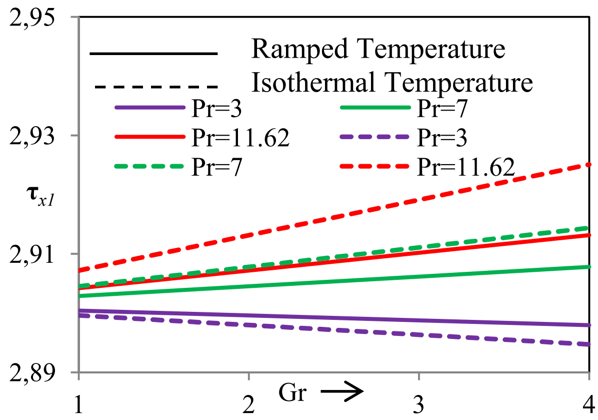

Fig.17. Shear stress at the moving plate with various values of 'Pr' against the values of 'Gr' due to primary velocity profiles.

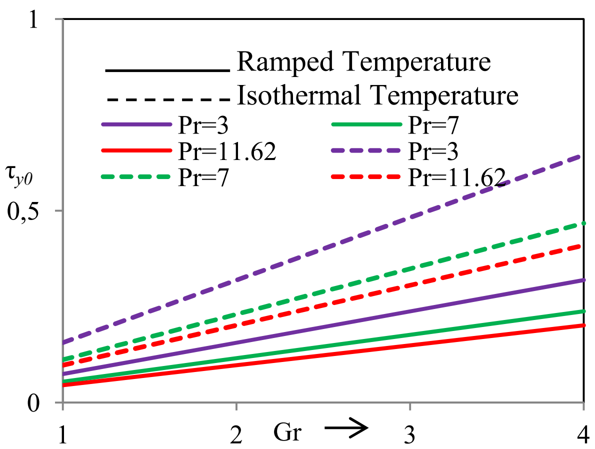

Fig.18. Shear stress at the stationary plate with various values of 'Pr' against the values of 'Gr' due to secondary velocity profiles.

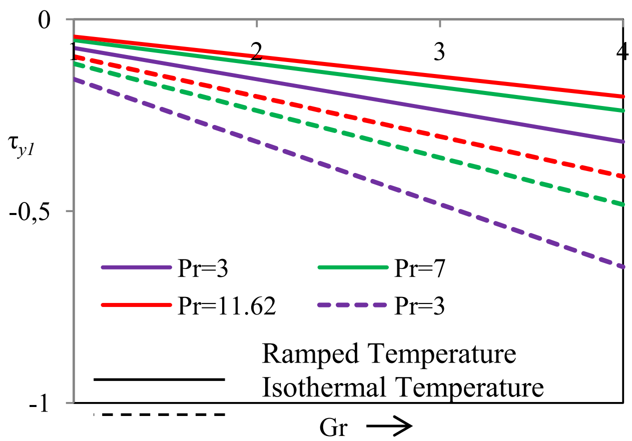

Fig.19. Shear stress at the moving plate with various values of 'Pr' against the values of 'Gr' due to secondary velocity profiles.

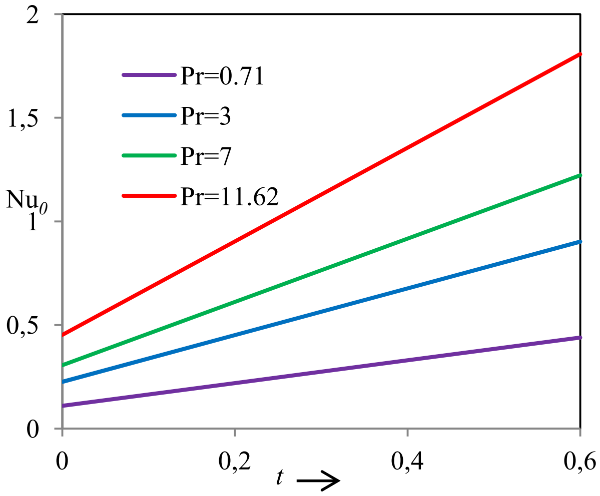

Fig.20. Rate of heat transfer at the stationary plate with various values of ‘Pr’ against the values of time ‘t’.

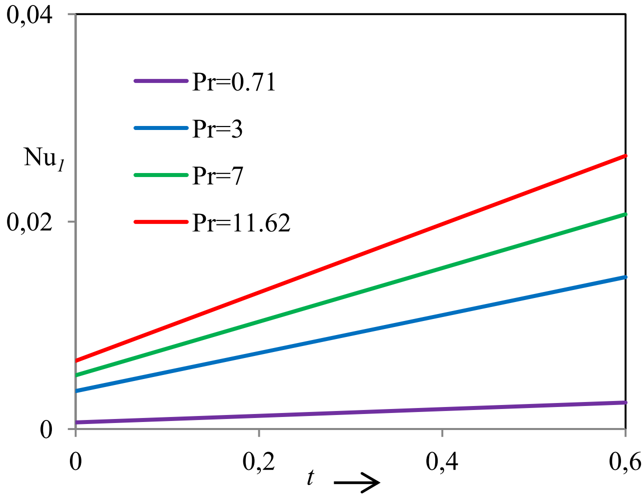

Fig.21. Rate of heat transfer at the moving plate with various values of ‘Pr’ against the values of time ‘t.

Figures 18 and 19 show the shear stress at the stationary plate $\left(\tau_{y_0}\right)$ and moving plate $\left(\tau_{y_1}\right)$ with various values of ‘Pr’ against the values of ‘Gr’ due to the secondary velocity for both ramped temperature and isothermal conditions. τ_{y_0} increases with increasing values of ‘Gr’ and decreases with increasing values of ‘Pr’. τ_{y_1} increases with increasing values of ‘Pr’ and decreases with increasing values of ‘Gr’ for both ramped temperature and isothermal conditions. Figures 20 and 21, show the rate of heat transfer coefficients Nu_0 and Nu_1 with the effect of Pr and time t near the stationary and moving plate respectively. Nu_0 and Nu_1 increase with increasing values of time t and Pr. Table 2 shows a comparison of skin friction results due to primary and secondary velocity near the stationary plate with the effect of magnetic parameter and the absence of Grashof number with $\Omega^2 = 15$ at time $t = 0.001$. The skin friction coefficient τ_{x_0} decreases and τ_{y_0} increases with increasing values of the magnetic parameter. The present results are in excellent agreement with the analytical solution.

Table 2. Comparison of skin friction results with existing results ($\Omega^2 = 15$ at time $t = 0.001$).

M^2	LTT (by Das *et al.* [22])		FEM (present results)	
	τ_{x0}	$-\tau_{y0}$	τ_{x0}	$-\tau_{y0}$
5	*0.213420*	*0.544380*	*0.2123922*	*0.5473171*
10	*0.178385*	*0.303637*	*0.1701235*	*0.3157638*
15	*0.132724*	*0.177382*	*0.1351722*	*0.1781934*
20	*0.095962*	*0.108245*	*0.0961279*	*0.1097895*

6. Conclusions

A FEM was employed to find the numerical solutions of the dimensionless governing coupled partial differential equations with suitable boundary conditions for the primary, secondary velocity and temperature of water at $4^{o}C$ as well as shear stresses and rate of heat transfer for ramped temperature and isothermal plates, in both cases the following conclusions are drawn from the above study

1. The primary velocity of the fluid increases with the increase of ‘Gr’ and decreases with the increase of ‘M^2’, ‘Ω^2’ and ‘Pr’.
2. The secondary velocity of the fluid increases with the increase of ‘Gr’ and decreases with the increase of ‘M^2’ and ‘Pr’. .
3. The temperature of the fluid increases with an increase of time and decreases with increasing values of ‘Pr’.
4. Shear stress at the stationary plate due to primary velocity increases with increasing values of ‘Gr’ and decreases with increasing values of ‘Ω^2’, ‘Pr’ and M^2’.
5. Shear stress at the moving plate due to primary velocity increases with increasing values of ‘Gr’, ‘Pr’, ‘Ω^2’ while decreases with increasing values of ‘M^2’.
6. Shear stress at the stationary plate due to secondary velocity increases with increasing values of ‘Gr’ and ‘Ω^2’ and decreases with increasing values of ‘Pr’ and ‘M^2’.
7. Shear stress at the moving plate due to secondary velocity increases with increasing values of ‘M^2’ and decreases with increasing values of ‘Pr’, ‘Ω^2’ and ‘M^2’.
8. At the stationary plate and moving plate the rate of heat transfer increases with increasing values of ‘Pr’ and time ‘t’.

Nomenclature

B_0 – external magnetic field
d – distance between the two plates (m)
Gr – Grashof number for heat transfer
g – acceleration due to gravity $\left(m\ s^{-2}\right)$
M^2 – dimensionless magnetic field parameter
Nu_0 – Nusselt number at the stationary plate
Nu_1 – Nusselt number at the moving plate
Pr – Prandtl number
T' – temperature of the fluid (K)
T'_w – temperature of the fluid at the lower plate (K)
T'_d – temperature of the fluid at the upper plate (K)
t – dimensionless time (s)
t' – dimensional time (s)
U – uniform velocity at the moving plate $\left(m\ s^{-1}\right)$
u – dimensionless primary velocity along the x-axis $\left(m\ s^{-1}\right)$
u' – velocity of the fluid in the x' - direction $\left(m\ s^{-1}\right)$
w – dimensionless secondary velocity along the y-axis $\left(m\ s^{-1}\right)$
w' – velocity of the fluid in the y' direction $\left(m\ s^{-1}\right)$
x' – co-ordinate axis along the lower stationary plate (m)
y' – co-ordinate axis normal to the $x'z'$ plane
z' – co-ordinate axis normal to the x'-axis
β – volumetric coefficient of thermal expansion $\left(K^{-1}\right)$
η – dimensionless displacement (m)
θ – dimensionless temperature (K)
κ – thermal conductivity of the fluid $\left(W\ m^{-1}K^{-1}\right)$

ν – kinematic viscosity $\left(m^2\ s^{-1}\right)$

ρ – density of the fluid $\left(Kg\, m^{-3}\right)$

σ – electric conductivity $\left(S\ m^{-1}\right)$

τ_{x_0} – shear stress at the stationary plate due to primary velocity $\left(N\ m^{-2}\right)$

τ_{x_1} – shear stress at the moving plate due to primary velocity $\left(N\ m^{-2}\right)$

τ_{y_0} – shear stress at the stationary plate due to secondary velocity $\left(N\ m^{-2}\right)$

τ_{y_1} – shear stress at the moving plate due to secondary velocity $\left(N\ m^{-2}\right)$

Ω' – angular velocity $\left(m\ s^{-1}\right)$

Ω^2 – dimensionless rotation parameter

References

[1] Forbes R.E. and Cooper J.W. (1975): *Natural convection in a horizontal layer of water cooled from above to near freezing*. – Journal of Heat Transfer, vol.97, pp.47-53.

[2] Goren S. (1966): *On free convection in water at 4°C*. – Chemical Engineering Science, vol.21, No.6-7, pp.515- 518.

[3] Lankford K.E. and Bejan A. (1986): *Natural convection in a vertical enclosure filled with water near 4°C*. – Journal of Heat Transfer, vol.108, pp.755-763.

[4] Khan W. and Gorla R. (2010): *Nonsimilar solutions for mixed convection of water at 4°C over a vertical surface with prescribed surface heat flux in a porous medium*. – Journal of Porous Media, vol.13, pp.1025-1032.

[5] Khan W. and Gorla R. (2011): *Mixed convection of water at 4°C along a wedge with variable surface temperature in a porous medium*. – International Journal of Thermo-Physics, vol.32, No.10, pp.2079-2091.

[6] Gorla R.S.R. and Stratman R.A. (1986): *Axisymmetric free convection boundary layer flow of water at 4°C past slender bodies*. – International Journal of Heat and Fluid Flow, vol.7, pp.179-183.

[7] Guedda M., Aly E. and Quahsine A. (2011): *Analytical and ChPDM analysis of MHD mixed convection over a vertical flat plate embedded in a porous medium filled with water at 4°C*. – Applied Mathematical, vol.35, No.10, pp.5182-5197.

[8] Xenos M., Dimas S. and Raptis A. (2013): *MHD free convective flow of water near 4°C past a vertical moving plate with constant suction*. – Applied Mathematics, vol.4, pp.52-57.

[9] Sharma P.R., Singh G. and Chamkha A.J. (2012): *Steady mixed convection flow of water 4°C at along a non-isothermal vertical moving plate with transverse magnetic field*. – Int. J. Industrial Mathematics, vol.4, No.3.

[10] Ramesh G.K., Gireesha B.J. and Gorla R.S.R. (2015): *Boundary layer flow past a stretching sheet with fluid-particle suspension and convective boundary condition*. – Heat and Mass Transfer, vol.51, No.8, pp 1061-1066.

[11] Gorla R.S.R. and Gireesha B.J. (2015): *Dual solutions for stagnation-point flow and convective heat transfer of a Williamson nanofluid past a stretching/shrinking sheet*. – Heat and Mass Transfer, pp.1-10.

[12] Darvishi M.T., Gorla R.S.R. and Khani F. (2014): *Unsteady thermal response of a porous fin under the influence of natural convection and radiation*. – Heat and Mass Transfer, vol.50, No.9, pp.1311-1317.

[13] Gireesha B.J., Mahanthesh B., Gorla R.S.R. and Manjunatha P.T. (2015): *Thermal radiation and Hall effects on boundary layer flow past a non-isothermal stretching surface embedded in porous medium with non-uniform heat source/sink and fluid-particle suspension*. – Heat and Mass Transfer, pp.1-15.

[14] Mukhopadhyay S. and Gorla R.S.R. (2012): *Effects of partial slip on boundary layer flow past a permeable exponential stretching sheet in presence of thermal radiation*. – Heat and Mass Transfer, vol.48, No.10, pp.1773-1781.

[15] Siddiqa S., Md. Hossain A. and Gorla R.S.R. (2015): *Conjugate natural convection flow over a vertical surface with radiation*. – Heat and Mass Transfer, pp.1-10.

[16] Singh A.K. and Gorla R.S.R. (2009): *Free convection heat and mass transfer with Hall current, Joule heating and thermal diffusion*. – Heat and Mass Transfer, vol.45, No.11, pp.1341-1349.

[17] Mukhopadhyay S., Mondal I.C. and Gorla R.S.R. (2012): *Effects of thermal stratification on flow and heat transfer past a porous vertical stretching surface*. – Heat and Mass Transfer, vol.48, No.6, pp.915-921.

[18] Bakier A.Y. and Gorla R.S.R. (2011): *Effects of thermophoresis and radiation on laminar flow along a semi-infinite vertical plate*. – Heat and Mass Transfer, vol.47, No.4, pp.419-425.

[19] Mohammadein A.A., Aissa W.A. and Gorla R.S.R. (2008): *The effect of radiation on mixed convection flow past a stretching surface*. – Heat and Mass Transfer, vol.44, No.9, pp.1035-1040.

[20] Kearsley A.J. (1994): *A steady state model of Couette flow with viscous heating*. – Int. J. Eng. Tech. Research, vol.32, pp.179-186.

[21] Singh A.K. (1988): *Natural convection in unsteady Couette motion*. – Defence Science Journal, vol.38, No.1, pp.35-41.

[22] Das S., Maji S.L., Guria M. and Jana R.N. (2009): *Unsteady MHD Couette flow in a rotating system*. – Mathematical and Computer Modelling, vol.50, pp.1211-1217.

[23] Singh K.D., Gorla M.G. and Hansraj (2005): *A periodic solution of oscillatory Couette flow through a porous medium in rotating system*. – Ind. J. Pure Appl. Math., vol.36, pp.151-159.

[24] Seth G.S., Sharma R., Kumari P. and Sarkar S. (2014): *Effects of Hall current and rotation on MHD Couette flow of class-II in the presence of an inclined magnetic field*. – J. Nature Sci. Sustainable Tech., vol.8, pp.27-50.

[25] Seth G.S., Prashant Kumar M. and Sharma R. (2015): *Hydromagnetic Couette flow of class-II and heat transfer through a porous medium in a rotating system with Hall effects*. – Journal of Mathematical Modeling, vol.3, No.1, pp.49-75.

[26] Victor M. Job, Sreedhara Rao Gunakala (2015): *Finite element analysis of unsteady radiative MHD natural convection Couette flow between permeable plates with viscous and joule dissipation*. – International Journal of Pure and Applied Mathematics, vol.99, No.2, pp.123-143.

[27] Anand Rao J., Sivaiah S. and Srinivasa Raju R. (2012): *Chemical reaction effects on an unsteady MHD free convection fluid flow past a semi-infinite vertical plate embedded in a porous medium with heat absorption*. – Journal of Applied Fluid Mechanics, vol.5, pp.63–70.

[28] Anand Rao J., Srinivasa Raju R. and Sivaiah S. (2012): *Finite element solution of heat and mass transfer in MHD flow of a viscous fluid past a vertical plate under oscillatory suction velocity*. – Journal of Applied Fluid Mechanics, vol.5, pp.1–10.

[29] Anand Rao J., Srinivasa Raju R. and Sivaiah S. (2012): *Finite element solution of MHD transient flow past an impulsively started infinite horizontal porous plate in a rotating fluid with Hall current*. – Journal of Applied Fluid Mechanics, vol.5, pp.105–112.

[30] Siva Reddy Sheri and Srinivasa Raju R. (2015): *Soret effect on unsteady MHD free convective flow past a semi–infinite vertical plate in the presence viscous dissipation*. – International Journal of Computational Methods in Engineering Science and Mechanics, vol.16, pp.132–141.

[31] Siva Reddy Sheri and Srinivasa Raju R. (2015): *Transient MHD free convective flow past an infinite vertical plate embedded in a porous medium with viscous dissipation*. – Meccanica, pp.1–12 (In Press).

[32] Sivaiah S. and Srinivasa Raju R. (2013): *Finite element solution of heat and mass transfer flow with hall current, heat source and viscous dissipation*. – Applied Mathematics and Mechanics (English Edition), vol.34, pp.559–570.

[33] Srinivasa Raju R. (2015): *Combined influence of thermal diffusion and diffusion thermo on unsteady hydromagnetic free convective fluid flow past an infinite vertical porous plate in presence of chemical reaction*. – Journal of Institution of Engineers (India): Series C (In Press).

[34] Srinivasa Raju R., Sudhakar K. and Rangamma M. (2013): *The effects of thermal radiation and heat source on an unsteady MHD free convection flow past an infinite vertical plate with thermal-diffusion and diffusion-thermo*. – Journal of Institution of Engineers (India): Series C, vol.94, pp.175–186.

[35] Ramana Murthy M.V., Srinivasa Raju R. and Anand Rao J. (2015): *Heat and mass transfer effects on MHD natural convective flow past an infinite vertical porous plate with thermal radiation and Hall Current*. – Procedia Engineering Journal, vol.127, pp.1330-1337.

[36] Rao V.S., Babu L.A. and Raju R.S. (2013): *Finite element analysis of radiation and mass transfer flow past semi-infinite moving vertical plate with viscous dissipation*. – Journal of Applied Fluid Mechanics, vol.6, pp.321–329.

[37] Hansbo A. and Hansbo P. (2004): *A finite element method for the simulation of strong and weak discontinuities in solid mechanics*. – Comp. Meth. Appl. Mech. Eng., vol.193, (33-35), 3523-3540.

[38] Clough R.W. (1960): *The finite element method in plane stress analysis*. – Proc. 2nd A.S.C.E. Conf. on Electronic Computation, Pittsburg, Pa.

[39] Rana P. and Bhargava R. (2011): *Numerical study of heat transfer enhancement in mixed convection flow along a vertical plate with heat source/sink utilizing nanofluids*. – Commun Nonlinear Sci. Numer. Simulat., vol.16, pp.4318–4334

[40] Fraeijs de Veubeke B. (2005): *Finite elements method in aerospace engineering problems*. – Computing Methods in Applied Sciences and Engineering Part 1 ,vol.10, pp.224-258.

[41] Tang Jiapeng, Xi Ping, Zhang Baoyuan, Hu Bifu (2013): *A finite element parametric modelling technique of aircraft wing structures*. – Chinese Journal of Aeronautics, vol.26, No.5, pp.1202–1210.

[42] Mahendran, Mahen, Siva Prasad N. and Sekar A.S. and Krishnapillai (2007): *Applications of finite element analysis in structural engineering*. – Proceedings International Conference on Computer Aided Engineering, pp.38-46, Chennai, India.

[43] Srinivasan K.R., Matouš K. and Geubelle P.H. (2008): *Generalized finite element method for modelling nearly incompressible biomaterial hyper elastic solids*. – Comput. Methods Appl. Mech. Engrg. 197, pp.4882–4893.

[44] Lin Y-Y. and Lo S-P. (2003): *Finite element modelling for chemical mechanical polishing process under different back pressures*. – J. Mat. Proc. Tech., vol.140, No.1-3, pp.646-652.

[45] Dettmer W. and Peric D. (2006): *A computational framework for fluid-rigid body interaction: finite element formulation and applications*. – Comp. Meth. Appl. Mech. Eng., vol.195, No.13-16, pp.1633-1666.

[46] John L. Volakis, Arindam Chatterjee and Leo C. Kempel (1998): *Finite element method electromagnetics: Antennas, microwave circuits, and Scattering Applications*. – Wiley-IEEE Press.

[47] Reece A.B.J. and Preston T.W. (2000): *Finite element methods in electrical power engineering*. – Oxford Science Publications.

[48] Bianchi N. (1999): *Electrical machine analysis using finite elements*. – Taylor and Francis.

[49] Charanjiv Gupta, Sanjay Marwaha and Manpreet Singh Manna (2009): *Finite element method as an aid to machine design: A Computational Tool*. – Excerpt from the Proceedings of the COMSOL Conference, Bangalore.

[50] Bathe K.J. (1996): *Finite element procedures*. – New Jersey: Prentice-Hall.

[51] Reddy J.N. (1985): *An introduction to the finite element method*. – New York: McGraw-Hill.

[52] Zienkiewicz O.C. (1971): *The finite element method in engineering science*. – 2nd edn., McGraw-Hill, New York.

Received: May 31, 2016
Revised: October 14, 2016